Photoproduction of $\Lambda^*(1405)$ with the N^* and the t-channel Regge contributions

Sang-Ho Kim,[1,*] Seung-il Nam,[2,1,†] Daisuke Jido,[3,‡] and Hyun-Chul Kim[4,5,§]

[1]*Asia Pacific Center for Theoretical Physics (APCTP), Pohang 37673, Republic of Korea*
[2]*Department of Physics, Pukyong National University (PKNU), Busan 608-737, Republic of Korea*
[3]*Department of Physics, Tokyo Metropolitan University, Hachioji, Tokyo 192-0397, Japan*
[4]*Department of Physics, Inha University, Incheon 402-751, Republic of Korea*
[5]*School of Physics, Korea Institute for Advanced Study (KIAS), Seoul 130-722, Republic of Korea*

We investigate the photoproduction of the $\Lambda(1405) \equiv \Lambda^*$ hyperon resonance, i.e., $\gamma p \to K^+ \Lambda^*$, employing the effective Lagrangian approach with the t-channel Regge trajectories at tree level. We extensively explore the effects from the nucleon resonances in the vicinity of the threshold $\sqrt{s}_{\text{th}} \approx 1900$ MeV, i.e., $N^*(2000)$, $N^*(2030)$, $N^*(2055)$, $N^*(2095)$, and $N^*(2100)$, and observe that they are of great importance to reproduce the recent CLAS experimental data. Total and differential cross sections are given as numerical results and compared with the experimental data, in addition to the photon-beam asymmetry. The invariant-mass distributions for $\gamma p \to K^+ \pi^0 \Sigma^0$ via Λ^* are also extracted from the two-body process results, showing a qualitative agreement with the data. We also discuss the constituent-counting rule for the internal structure of Λ^*, resulting in that Λ^* appears to be different from a simple three-quark (uds) state.

I. INTRODUCTION

The structure of exotic hadrons, such as the tetraquarks, pentaquarks, and meson-baryon molecular states for instance, has been one of the most interesting topics over decades in terms of the strongly interacting systems, governed by quantum chromodynamics (QCD). Recent discoveries of those exotics can shed light on the new understanding of QCD at low energies. The mesons consisting of four quarks, i.e., tetraquark state, has been reported by the Belle collaboration and BESIII collaboration [1–7]. The LHCb collaboration observed signals for the heavy pentaquark state P_c^+ as well [8]. The meson-baryon molecular state for $\Lambda(1405) \equiv \Lambda^*$, rather than a simple three-quark (uds) one, was proposed first even before QCD was established by Dalitz and Tuan [9,10] and recently its properties have been investigated via the unitarized chiral dynamics [11–21] and supported recently by the lattice-QCD (LQCD) simulation by investigating the strange form factor of Λ^* [22]. The LQCD simulation also supports the meson-baryon molecular nature by investigating the strange form factor of Λ^* [22]. In addition to the studies of structure for the $\Lambda(1405)$, the relevant production mechanisms were investigated extensively as well in Refs. [23–26].

In the present work, we would like to investigate the photoproduction of Λ^*, i.e., $\gamma p \to K^+ \Lambda^*$, employing the effective Lagrangian approach with the K and K^* Regge

trajectories at tree level. We focus on the contributions from the nucleon resonances near the threshold, such as $N^*(2000, 5/2^+)$ and $N^*(2100, 1/2^+)$, which have been reported in the Particle Data Group (PDG) [27]. In addition to them, a few missing resonances, i.e., $N^*(2030, 1/2^-)$, $N^*(2055, 3/2^-)$, and $N^*(2095, 3/2^-)$, predicted by the relativistic SU(6) quark model [28,29], are also taken into account. The electromagnetic and strong couplings are determined from the presently available theoretical and experimental results. Especially, we used the chiral unitary model (ChUM) for the strong couplings for Λ^* [30], because we do not have much information for $g_{KN\Lambda^*}$ and $g_{K^*N\Lambda^*}$ from experiments. The couplings for the $KN^*\Lambda^*$ vertex are taken from the quark-model calculations [29]. In order to satisfy the Ward-Takahashi (WT) identity, we make use of the gauge-invariant prescription for the form factors in the invariant amplitude. We compute various physical observables: The total ($\sigma_{\gamma p \to K^+ \Lambda^*}$) and differential ($d\sigma_{\gamma p \to K^+ \Lambda^*}/d\cos\theta$, $d\sigma_{\gamma p \to K^+ \Lambda^*}/dt$) cross sections, the photon-beam asymmetry ($\Sigma_{\vec{\gamma} p \to K^+ \Lambda^*}$), the invariant mass plot ($d\sigma_{\gamma p \to K^+ \pi^0 \Sigma^0}/dM_{\pi^0 \Sigma^0}$) for Λ^*, and so on.

From the numerical results, we observe that the nucleon-resonance contributions are crucial to reproduce the experimental data from the CEBAF Large Acceptance Spectrometer at Jefferson laboratory (CLAS/Jlab) [31] for the total cross section near the threshold. Among the resonances, we find that $N^*(2000, 5/2^+)$ and $N^*(2100, 1/2^+)$ dominate the threshold region. As for the differential cross sections as a function of the outgoing K^+ angle (θ) in the center-of-mass (c.m.) frame, the nucleon resonances play an important role to produce the strength of the cross sections below $\sqrt{s} \equiv W \lesssim 2.2$ GeV as

*sangho.kim@apctp.org
†sinam@pknu.ac.kr
‡jido@tmu.ac.jp
§hchkim@inha.ac.kr

expected. As the production energy increases, the conventional nonresonant contributions dominate and enhance the forward peaking at $\cos\theta \approx 0$, due to the strong K-exchange contribution.

The t-dependent differential cross sections $(d\sigma_{\gamma p \to K^+ \Lambda^*}/dt)$ is computed for $W = (2.0 - 4.0)$ GeV, with the help of the Regge approach, which can extend a simple low-energy Born approximation into the higher energy beyond the resonance region [32]. As expected, the curves are obviously modified by the N^* contributions near threshold. At the same time, the photon-beam asymmetry is computed as a function of $\cos\theta$ for different energies and is found to be in the shape of a distorted $\sin 2\theta$ according to the competing K- and K^*-Regge contributions.

Assuming that the decay width of Λ^* is sufficiently narrow $(\Gamma_{\Lambda^*} \approx 50 \text{ MeV} \ll \Lambda_{\text{hadron}} \approx 1 \text{ GeV})$ and the interference between the Λ^* and other nonstrange mesons decaying into $K\bar{K}$ are negligible in the Dalitz process of $\gamma p \to K^+ \pi^0 \Sigma^0$, the differential cross section of $d\sigma_{\gamma p \to K^+ \pi^0 \Sigma^0}/dM_{\pi^0 \Sigma^0}$ can be obtained from a simple formula with $\Gamma_{\Lambda^* \to \pi\Sigma}$ and $\sigma_{\gamma p \to K^+ \Lambda^*}$, which is computed previously [25]. By doing this, the distribution as a function of invariant mass $M_{\pi^0 \Sigma^0}$ is drawn and compared with the data, showing a good agreement and supporting its successful application.

Finally, we investigate the constituent-counting rule (CCR). The CCR is a method to analyze the internal structure of the hadrons involved in the $2 \to 2$ reaction process by dimensional considerations of the reaction amplitude in terms of the quark and gluon propagators at the large angle as well as the high energy. Applying this to the present reaction process, we observe that the numerical result, i.e., $s^7 d\sigma/dt$ as a function of W, differs clearly from the three-quark state for Λ^*, although it does not lead to the concrete conclusion that the results support the five-quark state for Λ^*.

The present work is organized as follows: In Sec. II, theoretical framework is briefly explained. Numerical results and relevant discussions are given in Sec. III. The final section is devoted for summary.

II. THEORETICAL FRAMEWORK

In this section, we provide a brief explanation for the present theoretical framework. Basically, we employ tree-level Born approximation with effective Lagrangians for the interaction vertices and the Regge trajectories for the pseudoscalar (PS) and vector (V) meson exchanges in the t channel. In terms of the PS meson-baryon coupling scheme, the relevant Feynman diagrams for the $\gamma p \to K^+ \Lambda^*(1405)$ reaction process are drawn in Fig. 1, in which k_1 and p_1 stand for the four momenta for the incident photon and target proton, whereas k_2 and p_2 for the outgoing K^+ and recoiled $\Lambda^*(1405)$, respectively. As for the t-channel, we consider the K and K^* exchanges with
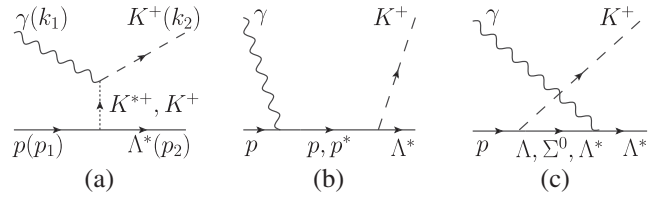

FIG. 1. Relevant tree-level Feynman diagrams for the $\gamma p \to K^+ \Lambda(1405)$ reaction process. p^*, Λ, Σ^0, and Λ^* stand for the proton resonances, $\Lambda(1116)$, $\Sigma^0(1193)$, and $\Lambda(1405)$, respectively.

their *Regge* propagators. By doing this, we can explore higher energy regions, which cannot be probed by the simple Born approximation [32]. The nucleon and its resonance states are taken into account for the baryon-pole diagrams in the s channel, whereas the hyperons, $\Lambda(1116)$, $\Sigma^0(1193)$, and $\Lambda(1405)$, are included for the u channel as shown in Fig. 1. Although there are other possible hyperon contributions in the u channel, such as $\Lambda(1520)$ and $\Lambda(1670)$ for instance, the magnetic transitions to $\Lambda(1405)$ have not been reported experimentally as well as theoretically. In addition, the u-channel resonances with a higher mass do not produce significant structure in the cross section in the energy region we are interested in. Hence, we will not take those higher-mass hyperons into account in the present calculation.

The effective Lagrangians for the EM interaction vertices read

$$\mathcal{L}_{\gamma KK} = -ie_K[K^\dagger(\partial_\mu K) - (\partial_\mu K^\dagger)K]A^\mu,$$

$$\mathcal{L}_{\gamma KK^*} = g_{\gamma KK^*}\epsilon^{\mu\nu\alpha\beta}\partial_\mu A_\nu[(\partial_\alpha K_\beta^{*-})K^+ + K^-(\partial_\alpha K_\beta^{*+})],$$

$$\mathcal{L}_{\gamma NN} = -\bar{N}\left[e_N\gamma_\mu - \frac{e\kappa_N}{2M_N}\sigma_{\mu\nu}\partial^\nu\right]A^\mu N,$$

$$\mathcal{L}_{\gamma\Lambda^*\Lambda^*} = \frac{e\mu_{\Lambda^*}}{2M_N}\bar{\Lambda}^*\sigma_{\mu\nu}\partial^\nu A^\mu\Lambda^*,$$

$$\mathcal{L}_{\gamma Y\Lambda^*} = \frac{e\mu_{\Lambda^* \to Y\gamma}}{2M_N}\bar{Y}\gamma_5\sigma_{\mu\nu}\partial^\nu A^\mu\Lambda^* + \text{H.c.}, \tag{1}$$

where A_μ, K, K^*, N, and Λ^* indicate the fields for the photon, pseudoscalar kaon, vector kaon, nucleon, and $\Lambda(1405)$, respectively. Y corresponds to the field for the ground-state Λ or Σ^0. M_h and e_h stand for the mass and electric charge of the hadron h, while e denotes the unit electric charge. As for the values for the coupling constants, the charged $g_{\gamma KK^*}^c$ is calculated from the experimental data for the decay width $\Gamma(K^* \to K\gamma)$, resulting in 0.254 GeV^{-1} [27]. The anomalous magnetic moment of the proton is given by $\kappa_N = 1.79$. The transition magnetic moments between two hyperons are also necessary and given by $\mu_{h \to h'}$. The SU(3) quark model gives $\mu_{\Lambda^*} = 0.44$ [33] which lies within the values predicted from the ChUM: $\mu_{\Lambda^*} = 0.2-0.5$ [34]. Meanwhile, we obtain $\mu_{\Lambda^* \to (\Lambda,\Sigma^0)\gamma} = (-0.43, 0.61)$ from an isobar model [35] to match the

K^-p atom data [36]. Thus, the output of the radiative decay widths is given by $\Gamma_{\Lambda^* \to \gamma\Lambda} = (27 \pm 8)$ keV and $\Gamma_{\Lambda^* \to \gamma\Sigma^0} = (23 \pm 7)$ keV [35] from the formula

$$\Gamma_{\Lambda^* \to \gamma Y} = \frac{(e\mu_{\Lambda^* \to \gamma Y})^2 \mathbf{k}^3}{4\pi M_N^2}, \tag{2}$$

derived from the $\gamma Y\Lambda^*$ Lagrangian in Eq. (1). Here $\mathbf{k}$ is the magnitude of the three-momentum of the hyperon Y in the rest frame of Λ^*.

The effective Lagrangians for the strong vertices are written by

$$\mathcal{L}_{KNY} = -ig_{KNY}\bar{N}\gamma_5 Y K + \text{H.c.},$$
$$\mathcal{L}_{KN\Lambda^*} = -ig_{KN\Lambda^*}\bar{N}\Lambda^* K + \text{H.c.},$$
$$\mathcal{L}_{K^*N\Lambda^*} = -g_{K^*N\Lambda^*}\bar{N}\gamma_5\gamma_\mu \Lambda^* K^{*\mu} + \text{H.c.} \tag{3}$$

Note that the strong coupling $g_{KN(\Lambda,\Sigma^0)}$ is given by $(-13.4, 4.09)$ from the Nijmegen soft-core potential (NSC97a) [37]. Because there is no sufficient experimental information on the strong coupling constants for the excited Λ hyperons, we resort to theoretical results, using the chiral-unitary model (ChUM) [30]. Averaging those theoretical values for various cases, we determine the strengths for the couplings for the numerical calculations as $|g_{KN\Lambda^*}| \simeq 1.95$ and $|g_{K^*N\Lambda^*}| \simeq 1.3$. All the values for the relevant couplings for the numerical calculations are summarized in Table I.

The invariant-scattering amplitude for the photoproduction can be written in general by

$$\mathcal{M} = I_h \bar{u}_{\Lambda^*} \mathcal{M}_h^\mu \epsilon_\mu u_N, \tag{4}$$

where u_N and u_{Λ^*} designate the Dirac spinors for the target nucleon and recoiled Λ^*, respectively, and ϵ_μ denotes the polarization vector of the incident photon. In the present calculation, the isospin factors are given by $I_K = I_N = I_{K^*} = I_\Lambda = I_{\Sigma^0} = I_{\Lambda^*} = 1$. The effective Lagrangians of Eqs. (1) and (3) being employed, the relevant hadronic amplitude ($\mathcal{M}_h^\mu$) besides the nucleon-resonance (N^*) contributions can be obtained straightforwardly as follows:

$$\mathcal{M}_K^\mu = -2ieg_{KN\Lambda^*}\frac{1}{t - M_K^2}k_2^\mu,$$

$$\mathcal{M}_N^\mu = -ieg_{KN\Lambda^*}\frac{\not{q}_s + M_N}{s - M_N^2}\left[\gamma^\mu + \frac{i\kappa_p}{2M_N}\sigma^{\mu\nu}k_{1\nu}\right],$$

$$\mathcal{M}_{K^*}^\mu = g_{\gamma KK^*}g_{K^*N\Lambda^*}\frac{1}{t - M_{K^*}^2}\epsilon^{\mu\nu\alpha\beta}\gamma_5\gamma_\nu k_{1\alpha}k_{2\beta},$$

$$\mathcal{M}_{\Lambda,\Sigma^0}^\mu = \frac{e\mu_{\Lambda^* \to \gamma(\Lambda,\Sigma^0)}}{2M_N}\frac{g_{KN(\Lambda,\Sigma^0)}}{u - M_{(\Lambda,\Sigma^0)}^2}\sigma^{\mu\nu}k_{1\nu}(\not{q}_u - M_{(\Lambda,\Sigma^0)}),$$

$$\mathcal{M}_{\Lambda^*}^\mu = \frac{e\mu_{\Lambda^*}}{2M_N}\frac{g_{KN\Lambda^*}}{u - M_{\Lambda^*}^2}\sigma^{\mu\nu}k_{1\nu}(\not{q}_u + M_{\Lambda^*}), \tag{5}$$

where $q_{s,t,u}$ stand for the off-shell four momenta, defined by $q_s = k_1 + p_1$, $q_t = k_1 - k_2$, and $q_u = p_2 - k_1$, and we also have $q_{s,t,u}^2 = (s, t, u)$, which denote the Mandelstam variables.

Considering the spatial extension of the hadrons, one needs to take into account the empirical form factors in the numerical calculations. We introduce a form factor as follows:

$$F = F(x) = \left[\frac{\Lambda^4}{\Lambda^4 + (x - M^2)^2}\right]^2. \tag{6}$$

Here, x and Λ indicate the Mandelstam variables and hadronic cutoff-mass parameter. Because the naive usage of the form factors can violate the Ward-Takahashi (WT) identity, various effective prescriptions to preserve the identity were suggested in Refs. [38–42]. The prescription from Ref. [41] being followed, the bare invariant amplitude is reconstructed with the form factors, satisfying the WT identity, as follows:

$$\epsilon \cdot \mathcal{M}_{\text{Born}} = \epsilon \cdot [(\mathcal{M}_K + \mathcal{M}_N)F_c + \mathcal{M}_{K^*}F_{K^*} + \mathcal{M}_\Lambda F_\Lambda$$
$$+ \mathcal{M}_{\Sigma^0}F_{\Sigma^0} + \mathcal{M}_{\Lambda^*}F_{\Lambda^*}], \tag{7}$$

where we define a common form factor as

$$F_c = F_{t,K} + F_{s,N} - F_{t,K}F_{s,N}, \tag{8}$$

which fulfills the on-mass-shell condition, i.e., the form factor becomes unity at $q_x^2 = m_h^2$, and the crossing symmetry. It is easy to verify that $k_\gamma \cdot \mathcal{M}_{\text{Born}} = k_1 \cdot \mathcal{M}_{\text{Born}} = 0$, i.e., satisfying the WT identity, as already shown in the previous works [23,25].

Now, we are in a position to consider the N^* contributions in the s channel. As shown in the previous work [25],

TABLE I. Relevant EM and strong coupling constants for the numerical calculations.

$g_{\gamma KK^*}^c$	κ_N	μ_{Λ^*}	$\mu_{\Lambda^* \to \gamma\Lambda}$	$\mu_{\Lambda^* \to \gamma\Sigma^0}$	$g_{KN\Lambda}$	$g_{KN\Sigma^0}$	$|g_{KN\Lambda^*}|$	$|g_{K^*N\Lambda^*}|$
−0.254/GeV	1.79 [27]	0.44 [33]	−0.43 [35,36]	0.61 [35,36]	−13.4 [37]	4.09 [37]	1.95 [30]	1.3 [30]

the nucleon resonance was found to be crucial to reproduce the experimental data. In the present work, we consider more resonances in the vicinity of the reaction threshold. Among the nucleon resonances listed in the Particle Data Group (PDG) [27], we take into account $N^*(2000, 5/2^+)$ and $N^*(2100, 1/2^+)$, which are near the reaction threshold and couple strongly to γN [27] as well as $K\Lambda^*$ [29] channels. Other resonances, for instance, $N^*(1895, 1/2^-)$, $N^*(1900, 3/2^+)$, $N^*(1990, 7/2^+)$, and $N^*(2060, 5/2^-)$, are excluded from our consideration, because their couplings to the $K\Lambda^*$ channel are very small or even exhibit zero values [29]. Meanwhile, the SU (6) relativistic-quark model provides us with missing resonances, such as $N^*(2030, 1/2^-)$, $N^*(2055, 3/2^-)$, and $N^*(2095, 3/2^-)$ [28,29]. Hence, five N^* states in total are taken into account in the present work. For this purpose, we first define the effective Lagrangians for the EM transitions for them with respect to their spin and parity (j^P) as follows:

$$\mathcal{L}_{\gamma NN^*}^{1/2\pm} = \frac{eh_1}{2M_N} \bar{N} \Gamma^\mp \sigma_{\mu\nu} \partial^\nu A^\mu N^* + \text{H.c.},$$

$$\mathcal{L}_{\gamma NN^*}^{3/2\pm} = -ie\left[\frac{h_1}{2M_N}\bar{N}\Gamma_\nu^\pm - \frac{ih_2}{(2M_N)^2}\partial_\nu\bar{N}\Gamma^\pm\right]F^{\mu\nu}N_\mu^* + \text{H.c.},$$

$$\mathcal{L}_{\gamma NN^*}^{5/2\pm} = e\left[\frac{h_1}{(2M_N)^2}\bar{N}\Gamma_\nu^\mp - \frac{ih_2}{(2M_N)^3}\partial_\nu\bar{N}\Gamma^\mp\right]\partial^\rho F^{\mu\nu}N_{\mu\rho}^*$$
$$+ \text{H.c.}, \tag{9}$$

where h_i^J denotes the EM transition coupling obtained from the Breit-Wigner helicity amplitudes A_i^J [27]. The explicit relations between them are given in Refs. [43,44]. Similarly, the effective Lagrangians for the strong interactions read

$$\mathcal{L}_{K\Lambda^*N^*}^{1/2\pm} = -ig_{K\Lambda^*N^*}\bar{K}\bar{\Lambda}^*\Gamma^\mp N^* + \text{H.c.},$$

$$\mathcal{L}_{K\Lambda^*N^*}^{3/2\pm} = \frac{g_{K\Lambda^*N^*}}{M_K}\partial^\mu\bar{K}\bar{\Lambda}^*\Gamma^\pm N_\mu^* + \text{H.c.},$$

$$\mathcal{L}_{K\Lambda^*N^*}^{5/2\pm} = \frac{ig_{K\Lambda^*N^*}}{M_K^2}\partial^\mu\partial^\nu\bar{K}\bar{\Lambda}^*\Gamma^\mp N_{\mu\nu}^* + \text{H.c.}, \tag{10}$$

where N^*, N_μ^*, and $N_{\mu\nu}^*$ denote the spin-1/2, −3/2, and −5/2 nucleon-resonance fields, respectively. To construct the nucleon resonances, whose spins are greater than 1/2, one needs a special description, such as the Rarita-Schwinger (RS) formalism [45,46]. In this formalism, there appear some theoretical uncertainties. In Refs. [47–50], the authors explored them by addressing the gauge invariant RS fields, off-shell effects, causality, etc. Although these subjects are interesting to study, it must be beyond our scope for the present research. Therefore, we make use of the simplest prescription for the RS fields as done in our previous work [51,52]. Note that we utilized the following notations depending on the parities of N^*s ($P = \pm$):

$$\Gamma^\pm = \begin{pmatrix} \gamma_5 \\ I_{4\times 4} \end{pmatrix}, \qquad \Gamma_\mu^\pm = \begin{pmatrix} \gamma_\mu\gamma_5 \\ \gamma_\mu \end{pmatrix}. \tag{11}$$

Using Eqs. (9) and (10), it is straightforward to compute the invariant amplitudes for the nucleon-resonance contributions with $\mathcal{M} = I_{N^*}\bar{u}_{\Lambda^*}\mathcal{M}_{N^*}u_N$ as in Eq. (4):

$$\mathcal{M}_{N^*}^{1/2\pm} = \mp g_{K\Lambda^*N^*}\frac{eh_1}{2M_N}\frac{\Gamma^\mp(\slashed{q}_s + M_{N^*})\Gamma^\mp}{s - M_{N^*}^2 + iM_{N^*}\Gamma_{N^*}}\sigma^{\mu\nu}k_{1\nu}\epsilon_\mu,$$

$$\mathcal{M}_{N^*}^{3/2\pm} = i\frac{g_{K\Lambda^*N^*}}{M_K}\frac{\Gamma^\pm k_2^\mu}{s - M_{N^*}^2 + iM_{N^*}\Gamma_{N^*}}\Delta_{\mu\nu}(q_s)$$
$$\times\left[\frac{eh_1}{2M_N}\Gamma_\lambda^\pm \mp \frac{eh_2}{(2M_N)^2}\Gamma^\pm p_{1\lambda}\right](k_1^\nu\epsilon^\lambda - k_1^\lambda\epsilon^\nu),$$

$$\mathcal{M}_{N^*}^{5/2\pm} = i\frac{g_{K\Lambda^*N^*}}{M_K^2}\frac{\Gamma^\mp k_2^\mu k_2^\nu}{s - M_{N^*}^2 + iM_{N^*}\Gamma_{N^*}}\Delta_{\mu\nu}^{\rho\sigma}(q_s)$$
$$\times\left[\frac{eh_1}{(2M_N)^2}\Gamma_\lambda^\mp \pm \frac{eh_2}{(2M_N)^3}\Gamma^\mp p_{1\lambda}\right]k_{1\sigma}(k_{1\rho}\epsilon^\lambda - k_1^\lambda\epsilon_\rho),$$
$$\tag{12}$$

where Γ_{N^*} stands for the full decay width for N^*. The spin-summation factor for spin-3/2 and spin-5/2 spinors are assigned by $\Delta_{\mu\nu}$ and $\Delta_{\mu\nu}^{\rho\sigma}$ and their explicit forms given by [43,44,53]

$$\Delta_{\mu\nu}(q) = (\slashed{q} + M_{N^*})\left[-g_{\mu\nu} + \frac{1}{3}\gamma_\mu\gamma_\nu + \frac{1}{3M_{N^*}}(\gamma_\mu q_\nu - \gamma_\nu q_\mu)\right.$$
$$\left. + \frac{2}{3M_{N^*}^2}q_\mu q_\nu\right],$$

$$\Delta_{\mu\nu}^{\rho\sigma}(q) = \slashed{q} + M_{N^*})\left[\frac{1}{2}(\bar{g}_\mu^\rho\bar{g}_\nu^\sigma + \bar{g}_\mu^\sigma\bar{g}_\nu^\rho) - \frac{1}{5}\bar{g}_{\mu\nu}\bar{g}^{\rho\sigma}\right.$$
$$\left. - \frac{1}{10}(\bar{\gamma}_\mu\bar{\gamma}^\rho\bar{g}_\nu^\sigma + \bar{\gamma}_\mu\bar{\gamma}^\sigma\bar{g}_\nu^\rho + \bar{\gamma}_\nu\bar{\gamma}^\rho\bar{g}_\mu^\sigma + \bar{\gamma}_\nu\bar{\gamma}^\sigma\bar{g}_\mu^\rho)\right]. \tag{13}$$

Here, we have used the following notations for convenience:

$$\bar{g}_{\mu\nu} = g_{\mu\nu} - \frac{q_\mu q_\nu}{M_{N^*}^2}, \qquad \bar{\gamma}_\mu = \gamma_\mu - \frac{q_\mu}{M_{N^*}^2}\slashed{q}. \tag{14}$$

The relevant input parameters from the PDG and missing nucleon resonances are summarized in Table II. The EM transition (h_i^J) and strong coupling $g_{K\Lambda^*N^*}$) constants are derived from the experimental [27] and theoretical information [28,29]. Note that we adopt the central ones among the values A_i^J and $G(\ell)$. The details for obtaining the strong coupling constants, $g_{K\Lambda^*N^*}$, are explained in the Appendix. Because the phase factors between the invariant amplitudes for different N^*s cannot be determined simply by symmetries, such as the gauge and flavor symmetries for instance, it is natural for them to be considered as free

TABLE II. The input parameters for the nucleon-resonance contributions. The helicity amplitudes $A_{1/2,3/2}$ $[10^{-3}/\sqrt{\text{GeV}}]$ are obtained from Refs. [27,28] and the decay amplitudes $G(\ell)$ $[\sqrt{\text{MeV}}]$ are extracted from Ref. [29].

	$A_{1/2}$	$A_{3/2}$	h_1	h_2	$G(\ell)$ [29]	$g_{K\Lambda*N*}$
$N^*(2000, 5/2^+)$ [27]	31 ± 10	-43 ± 8	-4.22	3.98	$-0.6^{+0.6}_{-1.6}$	-0.912
$N^*(2100, 1/2^+)$ [27]	10 ± 4	$\cdots$	-0.045	$\cdots$	$+5.2 \pm 0.8$	0.785
$N^*(2030, 1/2^-)$ [28]	20	$\cdots$	0.094	$\cdots$	$+1.2^{+0.9}_{-1.1}$	1.78
$N^*(2055, 3/2^-)$ [28]	16	0	-0.335	0.419	$+1.2^{+0.5}_{-0.9}$	-0.467
$N^*(2095, 3/2^-)$ [28]	-9	-14	0.018	-0.134	$+0.7^{+0.2}_{-0.4}$	-0.228

parameters to reproduce the data. In general, those amplitudes are represented by

$$\mathcal{M}_{\text{Res}} = \sum_{N^*} e^{i\psi_{N^*}} \mathcal{M}_{N^*} F_{N^*}, \qquad (15)$$

where ψ_{N^*} is a certain phase angle and F_{N^*} indicates the form factor, whose form is the same as $F(s)$ of Eq. (6). We note that, in Refs. [54–56], in order to suppress the nucleon-resonance contributions in the high-energy regions, the Gaussian form factors were employed. In describing the data, we, however, verified that our choice for the s-channel form factor in Eq. (6) works sufficiently to reproduce the data as shown in Sec. III. We reach a similar conclusion when the following Gaussian form factor is instead used with the same cutoff mass $\Lambda_{N^*} = 0.9$ GeV:

$$F_{\text{Gauss}}(s) = \exp\left\{-\frac{(s - M_{N^*}^2)^2}{\Lambda_{N^*}^4}\right\}. \qquad (16)$$

Although we would like to reproduce the data in the relatively low-energy region near the threshold, as done in the CLAS experiment, it is interesting to explore the higher-energy region theoretically for future experiments in the upgraded CLAS/Jlab and other experimental facilities. For this purpose, we employ the t-channel Regge trajectories for K and K^* mesons and follow closely Ref. [57]. In this Regge approach, the Feynman propagators in Eq. (5) are replaced simply by the Regge ones as

$$\frac{1}{t - M_K^2} \to P_K^{\text{Regge}} = \left(\frac{s}{s_0}\right)^{\alpha_K} \frac{\pi\alpha'_K}{\sin(\pi\alpha_K)} \left\{\begin{matrix} 1 \\ e^{-i\pi\alpha_K} \end{matrix}\right\} \frac{1}{\Gamma(1 + \alpha_K)},$$

$$\frac{1}{t - M_{K^*}^2} \to P_{K^*}^{\text{Regge}} = \left(\frac{s}{s_0}\right)^{\alpha_{K^*}-1} \frac{\pi\alpha'_{K^*}}{\sin(\pi\alpha_{K^*})} \left\{\begin{matrix} 1 \\ e^{-i\pi\alpha_{K^*}} \end{matrix}\right\} \frac{1}{\Gamma(\alpha_{K^*})}, \qquad (17)$$

where the Regge phases can be the constant (1) or the rotating ($e^{-i\pi\alpha_{K,K^*}}$) one. The Regge trajectories read [57]

$$\alpha_K = \alpha_K(t) = \frac{0.7}{\text{GeV}^2}(t - M_K^2),$$

$$\alpha_{K^*} = \alpha_{K^*}(t) = \frac{0.83}{\text{GeV}^2}t + 0.25, \qquad (18)$$

and we define the slope parameter as $\alpha'_{K,K^*} \equiv \partial\alpha_{K,K^*}(t)/\partial t$. Conventionally, the energy scale parameter is chosen to be $s_0 = 1$ GeV^2. With this in mind, the bare invariant amplitude of t and s channels in Eq. (7) is modified as

$$\epsilon \cdot \mathcal{M}_{t,s}^{\text{Regge}} = \epsilon \cdot [(\mathcal{M}_K + \mathcal{M}_N)(t - M_K^2)P_K^{\text{Regge}} + \mathcal{M}_{K^*}(t - M_{K^*}^2)P_{K^*}^{\text{Regge}}], \qquad (19)$$

for the present reaction process.

It is worth mentioning that the three-body (Dalitz) reaction process, $ab \to cde$, can be explored approximately in terms of the two-body one, if one assumes the following: (1) The decay widths for the decaying resonances are sufficiently narrow and (2) the interference between the different resonances in the Dalitz plot is negligible. If these conditions are fulfilled, one can write the differential cross section (invariant-mass plot) for the Dalitz process $\gamma p \to K^+ \pi^0 \Sigma^0$ as follows [25]:

$$\frac{d\sigma_{\gamma p \to K^+ \pi^0 \Sigma^0}}{dM_{\pi^0\Sigma^0}} \approx \frac{2M_{\Lambda^*}M_{\pi^0\Sigma^0}}{\pi} \frac{\sigma_{\gamma p \to K^+\Lambda^*}\Gamma_{\Lambda^* \to \pi^0\Sigma^0}}{(M_{\pi^0\Sigma^0}^2 - M_{\Lambda^*}^2)^2 + M_{\Lambda^*}^2\Gamma_{\Lambda^*}^2}, \qquad (20)$$

where $\sigma_{\gamma p \to K^+\Lambda^*}$ is the two-body total cross section. Here are some justifications for the usage of Eq. (20): First, the decay width of $\Lambda^* \to \pi\Sigma$ is about 50 MeV, which is much smaller than the typical energy range ~ 500 MeV in the present analysis. Therefore, condition (1) can be assumed to be reasonable. Second, in the Dalitz process $\gamma p \to K^+\pi^0\Sigma^0$, the Λ^* production interferes with the K^{+*} one on the Dalitz plot. Interestingly, in Ref. [58], it was found experimentally that the interference between the different resonant productions is almost negligible, although they focused on the different reactions process, i.e., $\gamma p \to K^+K^-p$. Hence, considering these observations, conditions (1) and (2) can be justified rather safely here, and we can use Eq. (20) for computing the Dalitz process

with the two-body cross section, which is computed by Eqs. (5) and (12). In doing this, the absolute value for the K^+ three momentum is obtained as a function of the invariant mass $M_{\pi^0\Sigma^0}$ as follows:

$$|\vec{k}_{K^+}| = \left[\left(\frac{s + M_{K^+}^2 - M_{\pi^0\Sigma^0}^2}{2W} \right)^2 - M_{K^+}^2 \right]^{\frac{1}{2}}. \quad (21)$$

Note that $|\vec{k}_{K^+}| = |\vec{k}_{\Lambda^*}|$ by construction in the c.m. frame.

As mentioned previously, the internal structure of Λ^* has been one of the most interesting subjects in the non-perturbative QCD. There have been several approaches to pin down the genuine structure of the hyperon resonance. Among various theoretical studies, we discuss the constituent-counting rule (CCR) [59,60]. Basically, in the CCR, the high-energy and large-angle scattering amplitudes for two-body processes, i.e., $ab \rightarrow cd$, are analyzed by dimensional considerations of the quark and gluon propagators, resulting in

$$\frac{d\sigma_{ab\rightarrow cd}}{dt} \propto \frac{1}{s^{n-2}}, \quad (22)$$

where n is the total number of the constituents of the particles involved in the scattering process. For instance, if Λ^* is composed of three quarks, the value of n becomes $1_\gamma + 3_N + 2_K + 3_{\Lambda^*} = 9$, whereas $n = 11$ for the five-quark system. Note that there are many uncertain theoretical ingredients, such as the distribution functions for the involved particles and so on, to apply the CCR to real problems of Λ^* [60]. It is, however, still valuable to test the relation in Eq. (22) with the present results, in which the Regge approach can extend the low-energy Born approximation to certain high energies beyond the resonance region.

III. NUMERICAL RESULTS AND DISCUSSIONS

In this section, we present the numerical results with corresponding discussions. Note that, in the present work, the free parameters are the sign of the coupling constants $g_{KN\Lambda^*}$ and $g_{K^*N\Lambda^*}$, the cutoff mass Λ in Eq. (6), the phase angle ψ_{N^*} in Eq. (15), and the Regge phases in Eq. (17). The cutoff masses are given in common for all the baryons as $\Lambda_{\Lambda,\Sigma,\Lambda^*,N^*} = 0.9$ GeV. Although the full-decay widths for the nucleon resonance, which appear in the denominator of the amplitudes in Eq. (12), are not free parameters as given in the PDG list [27], we fix it to be $\Gamma_{N^*} = 300$ MeV for all the resonances for brevity. We verified that about $\pm 10\%$ deviations in the widths do not make crucial differences in the qualitative consequences of the present work. The numerical results are given by using the constant and rotating Regge phases with the fitted parameters as listed in Table III to reproduce the CLAS/Jlab data.

Before performing the detailed calculations for reproducing the CLAS/Jlab experimental data, we would like to

TABLE III. Fitted parameter setups the constant and rotating Regge phases. See Eqs. (15) and (17) for details.

Regge phase	ψ_{N^*}	$g_{KN\Lambda^*}$	$g_{K^*N\Lambda^*}$
1 (constant)	$e^{i\pi/2}$	1.95	−1.3
$e^{-i\pi\alpha_{K,K^*}}$ (rotating)	$e^{i\pi}$	1.95	1.3

examine the effects of the nucleon-resonance contributions for the Λ^* photoproduction in a model-independent manner. Here we choose the constant Regge phase for simplicity. We consider a single resonance near the reaction threshold with different spin and parity, i.e. $N^*(2100, n/2^\pm)$ for a positive integer $n \leq 5$. For simplicity, we choose $\Gamma_{N^*} = 250$ MeV and $A_{1/2} = (3 \times 10^{-2})/\sqrt{\text{GeV}}$ for all the resonances. The reasons for those choices are as follows: (1) In the PDG list, the reported values for Γ_{N^*}s reside in (100–400) MeV with sizable uncertainties. Hence, the sort of a middle value is chosen. (2) Because we focus on the vicinity of the threshold, the h_2 contribution $\propto \partial N/M_{N^*}$ turns out to be small. Therefore, we only consider the h_1 contribution and the values of $A_{1/2}$ are in the order of $10^{-2}/\sqrt{\text{GeV}}$ as shown in the PDG list. Thus, similarly, the middle value is employed. In Fig. 2, six resonances are taken into account in total, depending on the spins and parities, and $g_{KN^*\Lambda^*}$ is fitted with the total cross section from the CLAS/Jlab data with the fixed h_1 values via the above $A_{1/2}$. As a result, the branching ratios of $\text{BR}_{n/2^\pm}$ are given as follows:

$$\text{BR}_{1/2^+} = 1.7 \times 10^{-2}, \qquad \text{BR}_{1/2^-} = 0.11,$$
$$\text{BR}_{3/2^+} = 9.5 \times 10^{-3}, \qquad \text{BR}_{3/2^-} = 4.0 \times 10^{-3},$$
$$\text{BR}_{5/2^+} = 2.1 \times 10^{-2}, \qquad \text{BR}_{5/2^-} = 5.9 \times 10^{-3}. \quad (23)$$

As the spin of N^* increases, the shapes of the angular distributions exhibit more fluctuations on their behaviors. We find that the nucleon resonances with $J^P = 1/2^+$, $3/2^+$, and $3/2^-$ more or less describe the CLAS/Jlab data within reasonable values of branching ratios, where $\text{BR} = \Gamma_{N^*\rightarrow K\Lambda^*}/\Gamma_{N^*}$ and $\Gamma_{N^*\rightarrow K\Lambda^*}$ is calculated from $g_{K\Lambda^*N^*}$ for each of the cases. But when more than a single resonance is considered simultaneously, we reach a different conclusion as we will see soon.

Now, let us show numerical results when employing our models. In the left panel of Fig. 3, we demonstrate the results for the total cross section for $\gamma p \rightarrow K^+\Lambda^*$ as a function of the photon laboratory energy E_{lab} by using the constant (thick lines) and rotating (thin lines) Regge phases as given in Table III. The experimental data are taken from the CLAS/Jlab collaboration [31]. The full result including the N^* (dot-dashed) and non-N^* (dashed) contributions is given in the solid line. It is worth mentioning that the peaklike bump around $E_{\text{lab}} = 2$ GeV is well reproduced by the nucleon resonances, whereas the non-N^* contribution
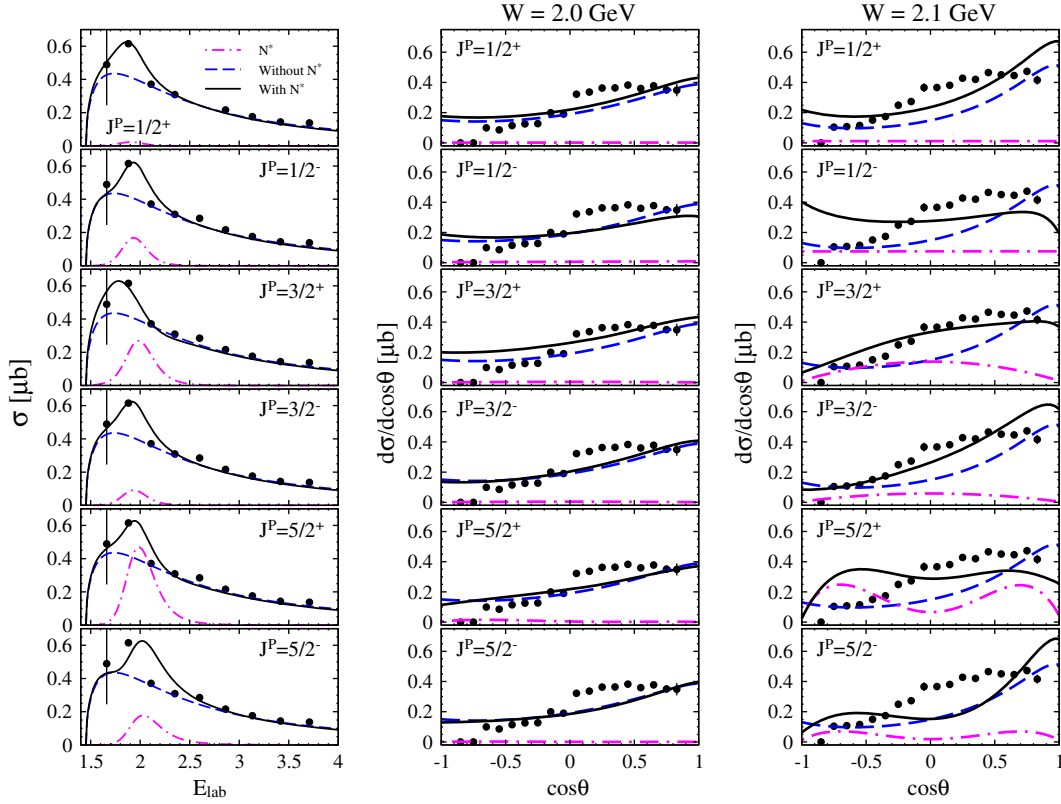
FIG. 2. Computed total and differential cross sections for six different spins and parities for nucleon resonances with $(M_{N^*}, \Gamma_{N^*}) = (2.1, 0.25)$ GeV.

curve decreases rapidly, due to the Regge propagators, as the energy increases. We also verified that the non-N^* contributions cannot reproduce the bump by changing form-factor types or their cutoff parameters. Moreover, by comparing the strengths of the N^* and total contributions, one can conclude that the constructive interference between the N^* and others plays an important role. As a consequence, within the most conventional tree-level approach like the present effective model, the nucleon resonances are crucial to explain the obvious cross-section enhancement near the threshold region for $\Lambda(1405)$

photoproduction. It is also interesting to see the separate effects from the different nucleon resonances. As shown there, after fitting the parameters to reproduce the data, the two Regge phases do not make obviously qualitative differences in the cross sections. Hence, in what follows, we will only use the constant Regge phase for the numerical calculations.

In the right panel of Fig. 3, we draw the total cross sections only from each resonance. It is clearly shown that $N^*(2000)$ and $N^*(2100)$ give dominant effects on the cross section, due to their relatively larger strong and EM
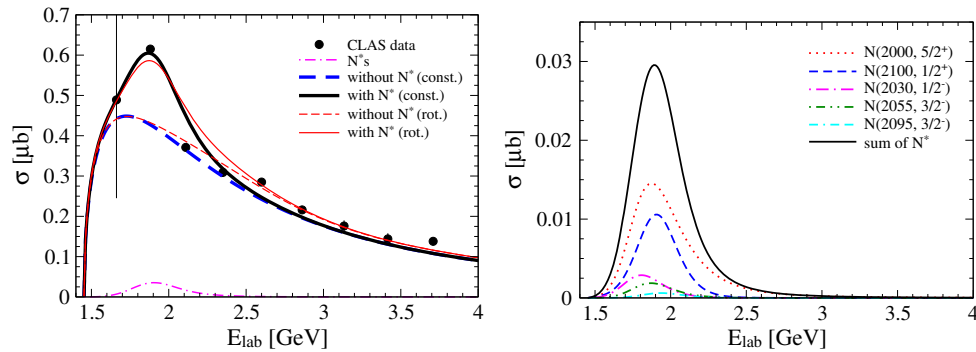

FIG. 3. Left: $\sigma_{\gamma p \to K^+ \Lambda^*}$ as a function of E_{lab}. The solid, dashed, and dot-dashed lines indicate the total, without N^*, and N^* contributions, respectively. The thick and thin lines correspond to the constant and rotating Regge phases for the K and K^* trajectories, respectively. The data are taken from Ref. [31]. Right: Separate contributions from various nucleon resonances.
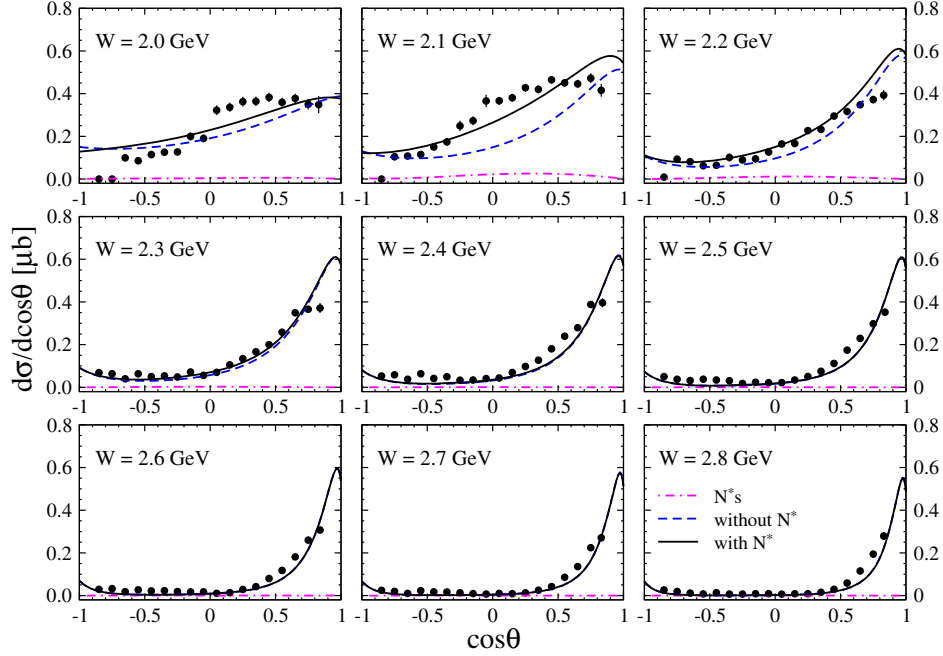
FIG. 4. $d\sigma_{\gamma p \to K^+ \Lambda^*}/d\cos\theta$ for different c.m. energies $W = (2.0\text{--}2.8)$ GeV. The data are taken from Ref. [31]. The legends are the same as those for the left panel of Fig. 3.

couplings than other resonances. In contrast, the missing resonances play only minor roles in producing the strength. The strong enhancement near the threshold region was already reported from the Laser Electron Photon Experiment at Super Proton ring-8 GeV (LEPS/SPring-8) [61]. The curve shape beyond the resonance region is reproduced mainly by the t-channel K-exchange contribution, in addition to the small but finite K^*-exchange one.

The numerical results for the angular dependence $d\sigma/d\cos\theta$ are drawn in Fig. 4 for different c.m. energies $W = (2.0\text{--}2.8)$ GeV. In overall, the full results (solid) show qualitatively good agreement with the data. We also observe that the forward-scattering enhancement becomes more obvious as the energy increases, due to the strong t-channel K exchange. At $W = 2.1$ GeV, it is found that the data are reproduced by the N^* and non-N^* contributions constructively. This observation agrees well with that shown in the total cross section. As the energy gets higher, the N^* contribution becomes diminished and almost flat as expected. At the same time, the small but sizable backward-scattering enhancement starts appearing gradually beyond $W = 2.3$ GeV. We verified that it originates mainly from the larger couplings in case of Λ and Σ^0 exchanges, i.e., $g_{KN(\Lambda,\Sigma^0)}$ and $\mu_{\Lambda^* \to (\Lambda, \Sigma^0)}$, in the u channel than other hyperons, as given in Table I.

Note that, quantitatively, in the low-energy region $W \leq 2.2$ GeV, we find sizable disagreement with the data for very backward angles $-1 \leq \cos\theta \leq -0.8$. Similar problems also take place in Refs. [47,48] for $K\Lambda$ photoproduction where the SU(3) symmetry limits on the Born coupling constants were considered. Although we anticipate that the unknown contributions beyond the present

model setup can resolve it, we will not make further detailed investigation on this issue in the present work and would like to leave it for the future. We verified that, even without our Regge approach, i.e., by using Eq. (7) rather than Eq. (19), we can obtain similar results for total and differential cross sections in the range of $E_{\text{lab}} \leq 4.0$ GeV. This is expected because our Regge model interpolates between low and high energy regions smoothly.

In the left panel of Fig. 5, we draw the numerical results for the differential cross sections $d\sigma/dt$ as a function of $-t' \equiv -(t - t_{\text{max}})$ for different c.m. energies $W = (2.0\text{--}4.0)$ GeV. The curves are computed with the N^* contributions and show a typical behavior of the momentum transfer. The slope is mostly determined by the dominant K Regge trajectory. The photon-beam asymmetry, i.e., the analyzing power, is one of the important physical quantities observed in hadron photoproductions. We define it as follows:

$$\Sigma_{\vec{\gamma} p \to K^+ \Lambda^*} = \frac{\frac{d\sigma}{d\Omega_\perp} - \frac{d\sigma}{d\Omega_\parallel}}{\frac{d\sigma}{d\Omega_\perp} + \frac{d\sigma}{d\Omega_\parallel}}, \qquad (24)$$

where the subscripts $\parallel$ and $\perp$ stand for the cases when the photon polarization vector is parallel and perpendicular to the reaction plane, respectively. In the case of unnatural parity exchange (K exchange), the perpendicular term in Eq. (24) is equal to zero, so $\Sigma_{\vec{\gamma} p \to K^+ \Lambda^*} = -1$, whereas natural parity exchange (K^* exchange) leads $\Sigma_{\vec{\gamma} p \to K^+ \Lambda^*}$ to positive values, since the corresponding perpendicular term dominates the parallel one. In the right panel of Fig. 5, we
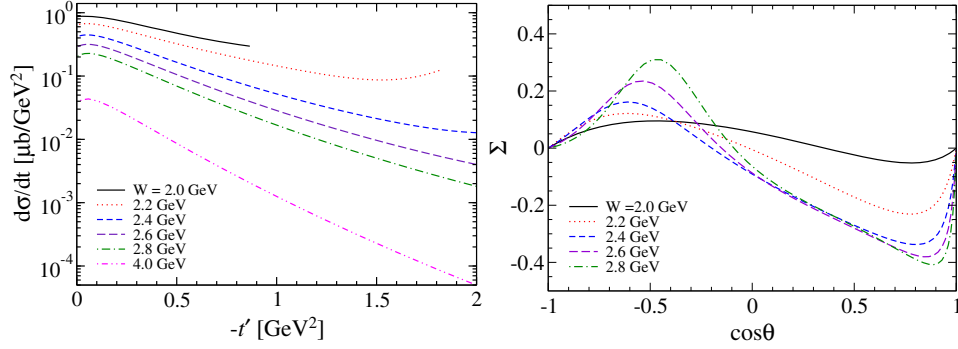
FIG. 5.　Left: $d\sigma_{\gamma p \to K^+ \Lambda^*}/dt$ as a function of $-t' \equiv -(t - t_{max})$ for different c.m. energies $W = (2.0$–$4.0)$ GeV. Right: $\Sigma_{\vec{\gamma} p \to K^+ \Lambda^*}$ as a function of $\cos \theta$ for different c.m. energies $W = (2.0$–$2.8)$ GeV.

present the numerical results for $\Sigma_{\vec{\gamma} p \to K^+ \Lambda^*}$ in the same manner with the left panel of Fig. 5 for different c.m. energies $W = (2.0$–$2.8)$ GeV. Note that the beam asymmetry becomes reversed around $\cos \theta \approx 0$, due to the competing K and K^* contributions. The effects of the N^*s turn out to be negligible. It is worth mentioning that the polarized quantity $\Sigma_{\vec{\gamma} p \to K^+ \Lambda^*}$ is very sensitive to the choice of the Regge phases for the t-channel strange-meson exchanges, because it is almost dominated by the Regge contributions. To confirm the effects of the Regge phases in the polarized physical quantities, one may need more reliable data to compare with.

In Fig. 6, we draw the invariant-mass distributions $d\sigma_{\gamma p \to K^+ \pi^0 \Sigma^0}/dM_{\pi^0 \Sigma^0}$ as a function of the invariant mass $M_{\pi^0 \Sigma^0}$ for different c.m. energies $W = (2.0$–$2.8)$ GeV, using Eq. (20) and the numerical results for the two-body

process, i.e., $\gamma p \to K^+ \Lambda^*$, given in Fig. 3. The theoretical curves describe the CLAS data [62] qualitatively well for all the energies, as expected from Eq. (20) by construction, due to the appropriate Breit-Wigner distribution and the strength from the two-body total cross section. From this observation, we find that the interference between the Λ^* and other vector-meson productions, such as K^*, on the Dalitz plot is practically small as given in Ref. [58]. In the low-energy region for $W \leq 2.2$ GeV, being similar to the total and differential cross sections as shown in Figs. 3 and 4, the nucleon resonances make considerable contributions to the invariant-mass distribution as well, as expected. We also observe that the nucleon resonance contributions becomes almost negligible beyond $W = 2.4$ GeV.

Finally, we would like to test the CCR for the present reaction process. For this purpose, we take $\theta = \pi/2$ in
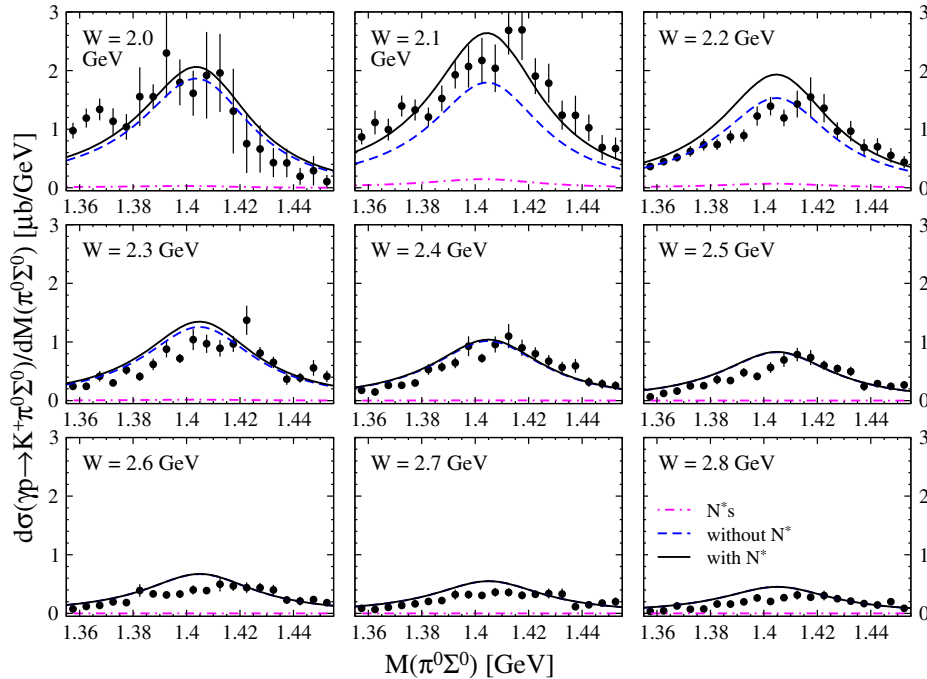

FIG. 6.　$d\sigma_{\gamma p \to K^+ \pi^0 \Sigma^0}/dM_{\pi^0 \Sigma^0}$ for different c.m. energies $W = (2.0$–$2.8)$ GeV. The data are taken from Ref. [62]. The legends are the same as those for the left panel of Fig. 3.
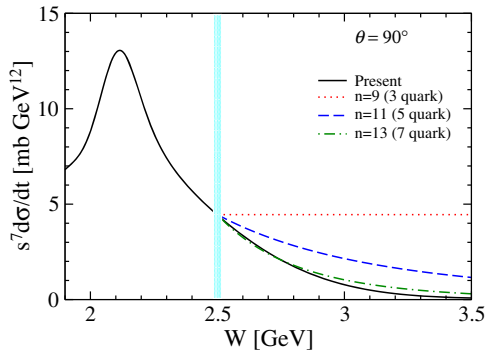
FIG. 7. $s^7 d\sigma_{\gamma p \to K^+ \Lambda(1405)}/dt$ as a function of $\sqrt{s} \equiv W$ at the angle $\theta = 90°$ for the case for $n = (9, 11, 13)$.

the c.m. frame as done in Refs. [59,60] and the numerical results are drawn in Fig. 7, where we draw $s^7 d\sigma/dt$ as a function of W. The solid curve stands for the full result with the nucleon resonances. Following the CCR, if Λ^* consists of three quarks as usual baryons, the resulting curve becomes flat (dotted), whereas it decreases with a tendency $\sim 1/W^4$ for the five-quark Λ^* (dashed) and $\sim 1/W^8$ for the seven-quark Λ^* (dot-dashed). Here, we assume that the resonance region is terminated at $W \approx 2.5$ GeV as observed in the invariant-mass plot in Fig. 6. The curves obviously exhibit a decreasing behavior with respect to W, and the slope matches with $\sim 1/W^8$, i.e., the seven-quark system for Λ^*. In Ref. [60], the CLAS/Jlab experimental data was fitted with $[s^{n-2}/f(\theta)]d\sigma/dt$ as a function of W, where $f(\theta)$ denotes a scattering-angle dependent function, and it showed that $n = (6.5–11.3)$, depending on energies, indicating that Λ^* is not a simple uds-quark state. Although the seven-quark state looks supported from the numerical results, it is still difficult to pin down the genuine structure of Λ^* from this observation, because we need to take into account more realistic information on the structure functions, energy-angular dependences, and so on in the CCR as well as in our model. Hence, we can conclude that, more or less, Λ^* is possibly distinctive from the simple uds-quark state, as far as we can reproduce the experimental data qualitatively well with the conventionally accepted model as in the present work.

IV. SUMMARY

We have investigated the photoproduction of $\Lambda(1405) \equiv \Lambda^*$, i.e., $\gamma p \to K^+ \Lambda^*$, by employing the effective Lagrangian with the Reggeized t-channel K and K^* exchanges at tree level. In addition to the ground state hadrons involved in the reactions process, we took five nucleon resonances near the reaction threshold into account. We performed numerical calculations for the energy and angular dependences of the cross section as well as the polarization observable, such as the photon beam asymmetry. The invariant-mass distribution for $\gamma p \to K^+ \pi^0 \Sigma^0$ was extracted from the two-body cross section

with some reasonable assumptions. Finally, the internal structure of Λ^* was explored by the constituent-counting rule (CCR), which provides the structure information of the hadrons in a reaction process in terms of the dimensional analyses of the scattering amplitudes at a large angle and high energies. Relevant results are summarized as follows:

(i) The nucleon resonances play an important role to reproduce the recent CLAS experimental data [31] near the threshold region. Especially, the so-called PDG resonances, $N^*(2000, 5/2^+)$ and $N^*(2100, 1/2^+)$, provide considerable contributions to the total cross section $\sigma_{\gamma p \to K^+ \Lambda^*}$, due to their relatively larger strong and EM couplings than other resonances, as far as we resort to available experimental and theoretical information to determine the couplings.

(ii) As expected, angular dependence, such as $d\sigma_{\gamma p \to K^+ \Lambda^*}/d\cos\theta$, is affected as well by the nucleon-resonance contributions in the low-energy region, whereas they get diminished as the energy increases. In overall, we observe strong forward-scattering enhancement, due to the t-channel K exchange. The numerical results for the $d\sigma_{\gamma p \to K^+ \Lambda^*}/dt$ are also given. We find that those results are affected by the inclusion of N^* resonances only near the threshold region $W \leq 2.2$ GeV.

(iii) Assuming some reasonable conditions, i.e., no interferences between the hyperon and vector-meson resonances on the Dalitz plot for instance, we draw the invariant-mass plot for $d\sigma_{\gamma p \to K^+ \pi^0 \Sigma^0}/dM_{\pi^0 \Sigma^0}$ in terms of the two-body cross section $\sigma_{\gamma p \to K^+ \Lambda^*}$ and the partial decay width $\Gamma_{\Lambda^* \to \pi\Sigma}$. Qualitatively, the experimental data of the CLAS collaboration are reproduced well for the considered energy regions. From this observation, we find that the interference between the Λ^* and K^* productions on the Dalitz plot must be practically small and it is consistent to the result of Ref. [58].

(iv) Finally, we examine the internal structure of Λ^* via the CCR. The calculated curve of $s^7 d\sigma_{\gamma p \to K^+ \Lambda^*}/dt$ as a function of the c.m. energy at $\theta = 90°$ shows a strong peaklike structure below $W \approx 2.5$ GeV and a rapid decrease beyond it, due to the nucleon resonances and the Reggeized t-channel contributions, respectively. Using the most simple parametrization of the scattering amplitude via the CCR, the slope of the calculated curve beyond the resonance region matches roughly with that for $n = 13$ from the relation $d\sigma/dt \propto 1/s^{n-2}$, which tells that Λ^* is a seven-quark state.

(v) However, because there are considerable theoretical uncertainties in this analysis, we can conclude safely that Λ^* is possibly different from the usual uds-quark state as reported in Ref. [60], if we take out results conservatively. Our numerical results for differential

cross sections match the CLAS data pretty well even at a large angle ($\theta = 90°$). Thus we believe that the results for $s^7 d\sigma/dt$ would be reliable to some extent even in relatively high-energy regions.

We want to mention that the photoproductions of the Λ, the Σ, and the $\Sigma(1385)$ baryons have been already investigated extensively by using similar approaches in the literature, i.e., the so-called Regge-plus-resonance framework [54–56,63]. Meanwhile, the electroproduction of Λ^* has its own interest, especially, as the CLAS collaboration recently has observed the Λ^* line shape in Λ^* electroproduction [64]. Although the relevant theoretical models appear in the literature [65], it is worth being studied within this effective model and related works are in progress. In summary, the present effective model approach with the Reggeized t-channel exchanges explains the Λ^* photoproduction qualitatively well, showing good agreement with the CLAS data. As discussed above, however, it is still difficult to determine the genuine internal structure of Λ^* within this simple model. Nonetheless, we have found a signal that Λ^* can be distinctive from usual three-quark baryons. More realistic studies with sophisticated form factors and Regge treatments are in progress and will appear elsewhere.

ACKNOWLEDGMENTS

APPENDIX COUPLING CONSTANTS AND DECAY AMPLITUDES

From the effective Lagrangians of Eq. (10), the partial decay width of nucleon resonance $N^*(j^P)$ into $K\Lambda^*$ can be calculated as

$$\Gamma[N^*(1/2^\pm) \to K\Lambda^*] = \frac{1}{4\pi} \frac{|\vec{q}|}{M_{N^*}} g^2_{K\Lambda^*N^*}(E_{\Lambda^*} \pm M_{\Lambda^*}),$$

$$\Gamma[N^*(3/2^\pm) \to K\Lambda^*] = \frac{1}{12\pi} \frac{|\vec{q}|^3}{M_{N^*}} \frac{g^2_{K\Lambda^*N^*}}{M_K^2}(E_{\Lambda^*} \mp M_{\Lambda^*}),$$

$$\Gamma[N^*(5/2^\pm) \to K\Lambda^*] = \frac{1}{30\pi} \frac{|\vec{q}|^5}{M_{N^*}} \frac{g^2_{K\Lambda^*N^*}}{M_K^4}(E_{\Lambda^*} \pm M_{\Lambda^*}).$$

$$\text{(A1)}$$

Here, the magnitude of the three-momentum and the energy for the Λ^* in the rest frame of the nucleon resonance reads

$$|\vec{q}| = \frac{1}{2M_{N^*}} \sqrt{[M_{N^*}^2 - (M_{\Lambda^*} + M_K)^2][M_{N^*}^2 - (M_{\Lambda^*} - M_K)^2]},$$

$$E_{\Lambda^*} = \sqrt{M_{\Lambda^*}^2 + |\vec{q}|^2}. \tag{A2}$$

We need to know how the effective Lagrangians are related to the decay amplitudes to obtain the coupling constants. The decay amplitude for $N^* \to K\Lambda^*$ can be expressed as follows [43]:

$$\langle K(\vec{q})\Lambda^*(-\vec{q}, m_f)| - i\mathcal{H}_{\text{int}}|N^*(\mathbf{0}, m_j)\rangle$$

$$= 4\pi M_{N^*} \sqrt{\frac{2}{|\vec{q}|}} \sum_{\ell, m_\ell} \left\langle \ell m_\ell \frac{1}{2} m_f | j m_j \right\rangle Y_{\ell, m_\ell}(\hat{q}) G(\ell), \quad \text{(A3)}$$

where $\langle \ell m_\ell \frac{1}{2} m_f | j m_j \rangle$ and $Y_{\ell, m_\ell}(\hat{q})$ are the Clebsch-Gordan coefficient and spherical harmonics, respectively. The relation between the partial wave decay amplitude $G(\ell)$ and the decay width $\Gamma(N^* \to K\Lambda^*)$ can be derived as

$$\Gamma(N^* \to K\Lambda^*) = \sum_\ell |G(\ell)|^2. \tag{A4}$$

The spin and parity of the nucleon resonance place constraints on the relative orbital angular momentum ℓ of the final state.

Let us first consider the case of a $j^P = \frac{1}{2}^+$ resonance. The relative orbital angular momentum is constrained by angular momentum and parity conservation such that $\ell = 0$ is possible, i.e., only s wave is allowed. In a similar way, for the decays of $j^P = (1/2^-, 3/2^-)$ resonances into $K\Lambda^*$, the final state is in the relative p wave, and for the resonances of $j^P = (3/2^+, 5/2^+)$ in the relative d wave. Finally, the $j^P = 5/2^-$ resonance allowed only f wave. Keeping this in mind, we can obtain the decay amplitudes in terms of the coupling constants for the decays of $j^P = (1/2^\pm, 3/2^\pm, 5/2^\pm)$ nucleon resonances into the $K\Lambda^*$ final state as follows:

$$G\left(\frac{1-P}{2}\right) = \sqrt{\frac{|\vec{q}|(E_{\Lambda^*} \pm M_{\Lambda^*})}{4\pi M_{N^*}}} g_{K\Lambda^*N^*} \text{ for } N^*(1/2^P),$$

$$G\left(\frac{3+P}{2}\right) = -\sqrt{\frac{|\vec{q}|^3(E_{\Lambda^*} \mp M_{\Lambda^*})}{12\pi M_{N^*}}} \frac{g_{K\Lambda^*N^*}}{M_K} \text{ for } N^*(3/2^P),$$

$$G\left(\frac{5-P}{2}\right) = \sqrt{\frac{|\vec{q}|^5(E_{\Lambda^*} \pm M_{\Lambda^*})}{30\pi M_{N^*}}} \frac{g_{K\Lambda^*N^*}}{M_K^2} \text{ for } N^*(5/2^P).$$

$$\text{(A5)}$$

[1] S. K. Choi *et al.* (Belle Collaboration), Observation of a Narrow Charmoniumlike State in Exclusive $B^\pm \to K^\pm\pi^+\pi^- J/\psi$ Decays, Phys. Rev. Lett. **91,** 262001 (2003).

[2] K. Abe *et al.* (Belle Collaboration), Observation of a Charmoniumlike Produced in Association with a J/ψ in e^+e^- Annihilation at $\sqrt{s} \approx 10.6$ GeV, Phys. Rev. Lett. **98,** 082001 (2007).

[3] S. K. Choi *et al.* (Belle Collaboration), Observation of a Resonancelike Structure in the $\pi^\pm\psi'$ Mass Distribution in Exclusive $B \to K\pi^\pm\psi'$ Decays, Phys. Rev. Lett. **100,** 142001 (2008).

[4] A. Bondar *et al.* (Belle Collaboration), Observation of Two Charged Bottomoniumlike Resonances in $\Upsilon(5S)$ Decays, Phys. Rev. Lett. **108,** 122001 (2012).

[5] M. Ablikim *et al.* (BESIII Collaboration), Observation of a Charged Charmoniumlike Structure in $e^+e^- \to \pi^+\pi^- J/\psi$ at $\sqrt{s} = 4.26$ GeVPhys. Rev. Lett. **110,** 252001 (2013).

[6] Z. Q. Liu *et al.* (Belle Collaboration), Charmoniumlike State at Belle, Phys. Rev. Lett. **110,** 252002 (2013).

[7] M. Ablikim *et al.* (BESIII Collaboration), Observation of a Charged Charmoniumlike Structure $Z_c(4020)$ and Search for the $Z_c(3900)$ in $e^+e^- \to \pi^+\pi^- h_c$, Phys. Rev. Lett. **111,** 242001 (2013).

[8] R. Aaij *et al.* (LHCb Collaboration), Observation of $J/\psi p$ Resonances Consistent with Pentaquark States in $\Lambda_b^0 \to J/\psi K^- p$ Decays, Phys. Rev. Lett. **115,** 072001 (2015).

[9] R. H. Dalitz and S. F. Tuan, A Possible Resonant State in Pion-Hyperon Scattering, Phys. Rev. Lett. **2,** 425 (1959).

[10] R. H. Dalitz and S. F. Tuan, The phenomenological representation of $\bar{k}$-nucleon scattering and reaction amplitudes, Ann. Phys. (N.Y.) **10,** 307 (1960).

[11] N. Kaiser, P. B. Siegel, and W. Weise, Chiral dynamics and the low-energy kaon-nucleon interaction, Nucl. Phys. **A594,** 325 (1995).

[12] E. Oset and A. Ramos, Nonperturbative chiral approach to S-wave anti-KN interactions, Nucl. Phys. **A635,** 99 (1998).

[13] J. C. Nacher, E. Oset, H. Toki, and A. Ramos, Photoproduction of the $\Lambda(1405)$ on the proton and nuclei, Phys. Lett. B **455,** 55 (1999).

[14] J. A. Oller and U. G. Meissner, Chiral dynamics in the presence of bound states: kaon-nucleon interactions revisited, Phys. Lett. B **500,** 263 (2001).

[15] D. Jido, E. Oset, and A. Ramos, Chiral dynamics of p wave in $K^- p$ and coupled states, Phys. Rev. C **66,** 055203 (2002).

[16] D. Jido, J. A. Oller, E. Oset, A. Ramos, and U. G. Meissner, Chiral dynamics of the two $\Lambda(1405)$ states, Nucl. Phys. **A725,** 181 (2003).

[17] S. i. Nam, H.-Ch. Kim, T. Hyodo, D. Jido, and A. Hosaka, Regularization dependence of $S = 0$ and $S = -1$ meson baryon system in the chiral unitary model, J. Korean Phys. Soc. **45,** 1466 (2004).

[18] M. F. M. Lutz and M. Soyeur, The associated photoproduction of positive kaons and $\pi^0\Lambda$ or $\pi\Sigma$ pairs in the region of the $\Sigma(1385)$ and $\Lambda(1405)$ resonances, Nucl. Phys. **A748,** 499 (2005).

[19] V. K. Magas, E. Oset, and A. Ramos, Evidence for the Two Pole Structure of the $\Lambda(1405)$ Resonance, Phys. Rev. Lett. **95,** 052301 (2005).

[20] T. Hyodo and D. Jido, The nature of the $\Lambda(1405)$ resonance in chiral dynamics, Prog. Part. Nucl. Phys. **67,** 55 (2012).

[21] M. Mai and U. G. Meißner, Constraints on the chiral unitary $\bar{K}N$ amplitude from $\pi\Sigma K^+$ photoproduction data, Eur. Phys. J. A **51,** 30 (2015).

[22] Y. Nemoto, N. Nakajima, H. Matsufuru, and H. Suganuma, Negative-parity baryon spectrum in quenched anisotropic lattice QCD, Phys. Rev. D **68,** 094505 (2003).

[23] S. i. Nam, J. H. Park, A. Hosaka, and H.-Ch. Kim, $\Lambda(1405, 1/2^-)$ photoproduction from the $\gamma p \to K^+\Lambda(1405)$ reaction, J. Korean Phys. Soc. **59,** 2676 (2011).

[24] S. X. Nakamura and D. Jido, $\Lambda(1405)$ photoproduction based on the chiral unitary model, Prog. Theor. Exp. Phys. **2014,** 023D01 (2014).

[25] S. i. Nam and H. K. Jo, Photoproduction of $\Lambda(1405)$ with the two-pole structure, arXiv:1503.00419.

[26] E. Wang, J. J. Xie, W. H. Liang, F. K. Guo, and E. Oset, Role of a triangle singularity in the $\gamma p \to K^+\Lambda(1405)$ reaction, Phys. Rev. C **95,** 015205 (2017).

[27] C. Patrignani *et al.* (Particle Data Group Collaboration), Review of particle physics, Chin. Phys. C **40,** 100001 (2016).

[28] S. Capstick, Photo- and electroproduction of nonstrange baryon resonances in the relativized quark model, Phys. Rev. D **46,** 2864 (1992).

[29] S. Capstick and W. Roberts, Strange decays of nonstrange baryons, Phys. Rev. D **58,** 074011 (1998).

[30] K. P. Khemchandani, A. Martinez Torres, H. Kaneko, H. Nagahiro, and A. Hosaka, Coupling vector and pseudoscalar mesons to study baryon resonances, Phys. Rev. D **84,** 094018 (2011).

[31] K. Moriya *et al.* (CLAS Collaboration), Differential photoproduction cross sections of the $\Sigma^0(1385)$, $\Lambda(1405)$, and $\Lambda(1520)$, Phys. Rev. C **88,** 045201 (2013); Publisher's Note, Phys. Rev. C **88,** 049902 (2013).

[32] A. Donnachie *et al.*, *Pomeron Physics and QCD* (Cambridge University Press, Cambridge, England, 2002).

[33] R. A. Williams, C. R. Ji, and S. R. Cotanch, Crossing and duality consistent study of Λ, Σ^0, and $\Lambda(1405)$ production by kaon photoproduction and radiative capture, Phys. Rev. C **43,** 452 (1991).

[34] D. Jido, A. Hosaka, J. C. Nacher, E. Oset, and A. Ramos, Magnetic moments of the $\Lambda(1405)$ and $\Lambda(1670)$ resonances, Phys. Rev. C **66,** 025203 (2002).

[35] H. Burkhardt and J. Lowe, Decays of the $K^- p$ atom and the $\Lambda(1405)$, Phys. Rev. C **44,** 607 (1991).

[36] D. A. Whitehouse, Radiative Kaon Capture at Rest on Hydrogen, Phys. Rev. Lett. **63,** 1352 (1989).

[37] V. G. J. Stoks and Th. A. Rijken, Soft-core baryon-baryon potentials for the complete baryon octet, Phys. Rev. C **59,** 3009 (1999).

[38] K. Ohta, Electromagnetic interactions of extended nucleons, Phys. Rev. C **40,** 1335 (1989).

[39] H. Haberzettl, Gauge invariant theory of pion photoproduction with dressed hadrons, Phys. Rev. C **56,** 2041 (1997).

[40] H. Haberzettl, C. Bennhold, T. Mart, and T. Feuster, Gauge-invariant tree-level photoproduction amplitudes with form factors, Phys. Rev. C **58,** R40 (1998).

[41] R. M. Davidson and R. Workman, Form-factors and photo-production amplitudes, Phys. Rev. C **63**, 025210 (2001).

[42] H. Haberzettl, X. Y. Wang, and J. He, Preserving local gauge invariance with t-channel Regge exchange, Phys. Rev. C **92**, 055503 (2015).

[43] Y. Oh, C. M. Ko and, and K. Nakayama, Nucleon and Δ resonances in $K\Sigma(1385)$ photoproduction from nucleons, Phys. Rev. C **77**, 045204 (2008).

[44] Y. Oh, Role of nucleon resonances in the $\pi N \to \omega N$ reaction, J. Korean Phys. Soc. **59**, 3344 (2011).

[45] W. Rarita and J. Schwinger, On a theory of particles with half integral spin, Phys. Rev. **60**, 61 (1941).

[46] L. M. Nath, B. Etemadi, and J. D. Kimel, Uniqueness of the interaction involving spin 3/2 particles, Phys. Rev. D **3**, 2153 (1971).

[47] J. C. David, C. Fayard, G. H. Lamot, and B. Saghai, Electromagnetic production of associated strangeness, Phys. Rev. C **53**, 2613 (1996).

[48] T. Mizutani, C. Fayard, G. H. Lamot, and B. Saghai, Off-shell effects in the electromagnetic production of strangeness, Phys. Rev. C **58**, 75 (1998).

[49] T. Vrancx, L. De Cruz, J. Ryckebusch, and P. Vancraeyveld, Consistent interactions for high-spin fermion fields, Phys. Rev. C **84**, 045201 (2011).

[50] S. Deser, V. Pascalutsa, and A. Waldron, Massive spin 3/2 electrodynamics, Phys. Rev. D **62**, 105031 (2000).

[51] S. H. Kim, S. i. Nam, Y. Oh, and H.-C. Kim, Contribution of higher nucleon resonances to $K^*\Lambda$ photoproduction, Phys. Rev. D **84**, 114023 (2011).

[52] S. H. Kim, S. i. Nam, A. Hosaka, and H.-C. Kim, $K^*\Sigma$ photoproduction off the proton target with baryon resonances, Phys. Rev. D **88**, 054012 (2013).

[53] F. A. Berends, J. W. van Holten, P. van Nieuwenhuizen, and B. de Wit, On field theory for massive and massless spin 5/2 particles, Nucl. Phys. **B154**, 261 (1979).

[54] T. Corthals, J. Ryckebusch, and T. Van Cauteren, Forward-angle $K^+\Lambda$ photoproduction in a Regge-plus-resonance approach, Phys. Rev. C **73**, 045207 (2006).

[55] T. Corthals, D. G. Ireland, T. Van Cauteren, and J. Ryckebusch, Regge-plus-resonance treatment of the $p(\gamma, K^+)\Sigma^0$ and $p(\gamma, K^0)\Sigma^+$ reactions at forward kaon angles, Phys. Rev. C **75**, 045204 (2007).

[56] L. De Cruz, J. Ryckebusch, T. Vrancx, and P. Vancraeyveld, Bayesian analysis of kaon photoproduction with the Regge-plus-resonance model, Phys. Rev. C **86**, 015212 (2012).

[57] M. Guidal, J. M. Laget, and M. Vanderhaeghen, Pion and kaon photoproduction at high-energies: Forward and intermediate angles, Nucl. Phys. **A627**, 645 (1997).

[58] S. Y. Ryu et al. (LEPS Collaboration), Interference Effect Between ϕ and $\Lambda(1520)$ Production Channels in the $\gamma p \to K^+ K^- p$ Reaction Near Threshold, Phys. Rev. Lett. **116**, 232001 (2016).

[59] H. Kawamura, S. Kumano, and T. Sekihara, Determination of exotic hadron structure by constituent-counting rule for hard exclusive processes, Phys. Rev. D **88**, 034010 (2013).

[60] W. C. Chang, S. Kumano, and T. Sekihara, Constituent-counting rule in photoproduction of hyperon resonances, Phys. Rev. D **93**, 034006 (2016).

[61] M. Niiyama et al., Photoproduction of $\Lambda(1405)$ and $\Sigma^0(1385)$ on the proton at $E_\gamma = 1.5$–2.4 GeV, Phys. Rev. C **78**, 035202 (2008).

[62] K. Moriya et al. (CLAS Collaboration), Measurement of the $\Sigma\pi$ photoproduction line shapes near the $\Lambda(1405)$, Phys. Rev. C **87**, 035206 (2013).

[63] J. He, $\Sigma(1385)$ photoproduciton from proton within a Regge-plus-resonance approach, Phys. Rev. C **89**, 055204 (2014).

[64] H. Y. Lu et al. (CLAS Collaboration), First observation of the $\Lambda(1405)$ line shape in electroproduction, Phys. Rev. C **88**, 045202 (2013).

[65] R. A. Williams, C. R. Ji, and S. R. Cotanch, Hyperon electroproduction in a crossing and duality constrained model, Phys. Rev. C **46**, 1617 (1992).